

Traveling planetary wave activity from mesopause region airglow temperatures determined by the Network for the Detection of Mesospheric Change (NDMC)

E.R. Reisin^{a,*}, J. Scheer^a, M.E. Dyrland^b, F. Sigernes^b, C.S. Deehr^c, C. Schmidt^d, K. Höppner^d, M. Bittner^d, P.P. Ammosov^e, G.A. Gavriljeva^e, J. Stegman^f, V.I. Perminov^g, A.I. Semenov^g, P. Knieling^h, R. Koppmann^h, K. Shiokawaⁱ, R.P. Lowe^j, M.J. López-González^k, E. Rodríguez^k, Y. Zhao^l, M.J. Taylor^l, R.A. Buriti^m, P.J. Espyⁿ, W.J.R. French^o, K.-U. Eichmann^p, J.P. Burrows^p, C. von Savigny^q

^a Instituto de Astronomía y Física del Espacio, CONICET-UBA, Buenos Aires, Argentina

^b Birkeland Centre of Space Science, University Centre in Svalbard, Longyearbyen, Norway

^c Geophysical Institute, University of Alaska Fairbanks, USA

^d Deutsches Zentrum für Luft- und Raumfahrt (DLR), Oberpfaffenhofen, Germany

^e Institute of Cosmophysical Research and Aeronomy SB RAS, Yakutsk, Russia

^f Meteorologiska Institutionen, Stockholms Universitet, Sweden

^g Obukhov Institute of Atmospheric Physics, Russian Academy of Sciences, Moscow, Russia

^h Physics Department, University of Wuppertal, Germany

ⁱ Solar-Terrestrial Environment Laboratory, Nagoya University, Japan

^j University of Western Ontario, London, Ontario, Canada

^k Instituto de Astrofísica de Andalucía, CSIC, Granada, Spain

^l Center for Atmospheric and Space Sciences, Utah State University, USA

^m Unidade Acadêmica de Física, Universidade Federal de Campina Grande, Paraíba, Brazil

ⁿ Norges Teknisk-Naturvitenskapelige Universitet, Trondheim, and Birkeland Centre for Space Science, Bergen, Norway

^o Australian Antarctic Division, Kingston, Tasmania, Australia

^p Institut für Umweltphysik, Universität Bremen, Bremen, Germany

^q Institut für Physik, Ernst-Moritz-Arndt Universität, Greifswald, Germany

ARTICLE INFO

Article history:

Received 25 April 2014

Received in revised form

16 June 2014

Accepted 9 July 2014

Available online 15 July 2014

Keywords:

Traveling planetary wave activity

Ground-based airglow observations

Rotational temperature

Network for the Detection of Mesospheric Change (NDMC)

ABSTRACT

The global distribution of traveling planetary wave (PW) activity in the mesopause region is estimated for the first time from ground-based airglow measurements. Monthly and total mean climatologies of PW power are determined from rotational temperatures measured at 19 sites from 78° N to 76° S which contribute to the Network for the Detection of Mesospheric Change (NDMC). Wave power is expressed as the standard deviation of nocturnal mean temperature around the seasonal temperature variation. The results from 20° N confirm the SABER traveling PW proxy by Offermann et al. (2009, *J. Geophys. Res.* 114, D06110) at two altitudes. Most sites between 69° S and 69° N show total mean traveling PW activity of about 6 K, and only some high latitude sites have considerably higher activity levels. At the two tropical sites, there is practically no seasonal variation of PW activity. At 70% of the midlatitude sites, the seasonal variation is moderate for most of the year, but it is quite appreciable at all high latitude sites. Results about traveling PW activity at 87 km and 95 km available from several sites signal similar behavior at both altitudes. The total mean climatological results here obtained have further been used to separate the traveling PW contribution from the superposition of wave types contained in OH rotational temperature fluctuations measured by the SCIAMACHY instrument on Envisat. A narrow equatorial wave activity maximum is probably caused by gravity waves, while a tendency towards greater activity at higher northern latitudes may be due to stationary planetary waves.

© 2014 Elsevier Ltd. All rights reserved.

* Corresponding author.

E-mail address: ereisin@iafe.uba.ar (E.R. Reisin).

1. Introduction

The term “planetary waves” (PWs) refers to global-scale atmospheric waves of different types (see Smith (2012, Section 4.4) and references therein). According to period, they can be divided into stationary (or quasi-stationary) PWs and traveling PWs. Stationary PWs have long been known in the lower and middle atmosphere and exhibit a pronounced seasonal pattern. Traveling PWs have periods between about 2 and 30 days. These include eastward and westward propagating PWs, but there are also zonally symmetric waves (see, e.g., Pancheva et al. (2009)), which we can look upon as traveling PWs of zonal wave number zero (although, strictly speaking, they do not travel).

Temperature measurements in the mesopause region (80 to 100 km) by airglow techniques are routinely done at night-time from a considerable number of ground stations, in the recent decades.

At these altitudes, traveling planetary waves are expected to be the dominant contribution to the quasi-periodic day-to-day variability of nocturnal mean temperatures. Stationary PWs should be invisible to ground-based airglow observations (except by higher-order effects due to temporal changes of amplitude or phase).

Most of the literature on PWs in the mesopause region focusses on certain periods (5 days, 10 days, 16 days, etc.) of traveling PW normal modes (e.g., Pancheva et al. (2009, 2010), and references therein). Other investigations have dealt with a certain frequency range (as empirically determined by spectral analysis of temperature time series), either at a fixed place (e.g., Espy et al. (1997), Bittner et al. (2000), French and Burns (2004), Buriti et al. (2005), Murphy et al. (2007), and López-González et al. (2009)), or a longitudinal chain of stations (e.g., Scheer et al. (1994) and Takahashi et al. (2006)).

Some studies arrive at a satisfactory identification of individual PW types and propagation modes by determining their period, amplitude, and wavenumber, with spectral analysis techniques (e.g., Pancheva et al. (2009), Scheer et al. (1994), and Takahashi et al. (2006)). However, it is unlikely that *all* the waves present are thus correctly identified. This is because of nonstationarity, wave transients, limited spectral resolution, etc. Nonstationarity also may lead to an underestimation of the amplitudes of waves which have been identified.

An alternative approach to PW study consists in determining PW power directly as a measure of integral PW activity based on the determination of the variance of suitably averaged temperatures (after subtracting the seasonal temperature variation). This approach combines greater informational economy with more robustness than can be obtained with spectral analysis techniques. It is insensitive to the inevitable deviations from stationarity, or from linearity, and obviates the need to identify and distinguish all the individual waves by period, phase, zonal wave number, and to determine their respective amplitudes. The information obtained by the variance approach is complementary to the information about individual PWs and cannot easily be derived otherwise.

Wave activity can also be expressed in terms of the standard deviation, i.e. the square root of variance, as has been done for mesopause region temperatures by Bittner et al. (2002). A proxy for the climatology of monthly mean traveling planetary wave activity for different altitudes and latitudes has recently been suggested by Offermann et al. (2009). That paper gives tables of monthly mean PW activity as standard deviations for three latitudes (20° N, 50° N, and 70° N), and at altitudes from 40 to 100 km, derived from temperature measurements by the SABER (Sounding of the Atmosphere using Broadband Emission Radiometry) instrument on the TIMED (Thermosphere Ionosphere Mesosphere Energetics and Dynamics) satellite. The technique used consisted of subtracting the contributions due to gravity

waves, stationary planetary waves, and tides from the observed temperature variance. The validity of this approach for the mesopause region could be tested at that time by comparison with ground-based airglow (rotational) temperatures from Wuppertal (Offermann et al., 2009).

In principle, integral PW power can also be determined from wind data as available with different radar techniques. A relatively recent example is given by Jacobi et al. (2008). Comparison with results of temperature measurements, while feasible in principle, would not be straightforward, since it strongly depends on mean temperature, and also on the vertical temperature profile (see, e.g., Offermann et al. (2009, Section 6.1)).

Here, we present the first estimation of the global distribution of integral traveling PW power from ground-based airglow data. Traveling PW climatologies are obtained from a joint data analysis of rotational temperatures acquired from many ground stations that now contribute to the global Network for the Detection of Mesospheric Change (NDMC, officially started in 2007 as “Network for the Detection of Mesopause Change”; see <http://wdc.dlr.de/ndmc/>). We shall also make use of the wave information contained in the OH rotational temperatures measured by the SCIAMACHY instrument on the Envisat satellite.

2. Data

Airglow temperatures from 19 NDMC sites were used, as listed in Table 1, sorted by latitude, with the NDMC 3-letter ID code and location name. For space reasons we abbreviate “Longyearbyen” for the “Kjell Henriksen Observatory” (KH1), “Schneefernerhaus” for “Umweltforschungsstation Schneefernerhaus” (UFS), “Delaware” for “Delaware Observatory” (DL1), “Sierra Nevada” for “Observatorio de Sierra Nevada” (OSN), “Cariri” for “Cariri Airglow Observatory” (CAR), and “Cerro Pachón” for “Andes Lidar Observatory” (ALO).

Table 1

Geographical distribution of the NDMC airglow instrument sites contributing to the present analysis.

ID	Short name	Latitude	Longitude	Layer	Reference
KH1	Longyearbyen	78.15° N	16.04° E	OH	Sigernes et al. (2003)
ALR	ALOMAR	69.28° N	16.01° E	OH	Bittner et al. (2010)
MAI	Maimaga	63.1° N	127.1° E	OH	Ammosov and Gavriljeva (2000)
STO	Stockholm	59.5° N	18.2° E	OH	Espy and Stegman (2002)
ZVE	Zvenigorod	55.69° N	36.77° E	OH	Khomich et al. (2008)
WUP	Wuppertal	51.25° N	7.15° E	OH	Bittner et al. (2002)
OPN	Oberpfaffenhofen	48.09° N	11.27° E	OH	Bittner et al. (2010)
UFS	Schneefernerhaus	47.42° N	10.98° E	OH	Bittner et al. (2010)
RIK	Rikubetsu	43.50° N	143.80° E	OH, O ₂	Shiokawa et al. (2007)
DL1	Delaware	42.87° N	81.38° W	OH	Lowe and Turnbull (1995)
OSN	Sierra Nevada	37.06° N	3.39° W	OH, O ₂	López-González et al. (2004)
STA	Sata	31.02° N	130.68° E	OH, O ₂	Shiokawa et al. (2007)
MA1	Maui	20.71° N	156.26° W	OH, O ₂	Taylor et al. (2001)
CAR	Cariri	7.38° S	36.53° W	OH	Buriti et al. (2004)
ALO	Cerro Pachón	30.25° S	70.74° W	OH	Taylor et al. (2001)
LEO	El Leoncito	31.80° S	69.29° W	OH, O ₂	Scheer and Reisin (2001)
ROT	Rothera	67.57° S	68.13° W	OH	Espy et al. (2003)
DAV	Davis	68.58° S	77.97° E	OH	Greet et al. (1998)
HAL	Halley	75.52° S	26.72° W	OH	Espy et al. (2003)

Northern latitudes from 78° to 31° are rather uniformly covered by 12 sites at an average spacing of 4°. Most of these are in longitudinal groups in Western and Central Europe, and three sites in East Asia. Farther south, latitudinal coverage is sparse, with two tropical, two lower midlatitude, and three high-latitude sites. For details about the sites, see <http://wdc.dlr.de/ndmc/>.

Rotational temperatures determined from one of the OH Meinel emission bands are available from all sites. These temperatures correspond to the kinetic temperature at a nominal altitude of 87 km. The small differences in effective emission height (by no more than about 2 km; see von Savigny et al. (2012a), and references therein) of the different OH bands observed are inconsequential for the present study. Five of the sites, identified in Table 1, also supply temperatures based on the O₂b (0–1) Atmospheric band (at 95 km nominal altitude). Emission height variations around the nominal altitudes by typically ± 2 km (as frequently reported for OH), and occasionally even greater deviations, are probably due to the vertical advection of the constituents responsible for the emissions. Under this view, the height variations are only part of the dynamical activity and so do not represent a problem for the study of waves (of whatever period) from airglow temperature variations.

Different types of grating spectrometers, Michelson interferometers, imaging or non-imaging filter instruments, and a tilting filter spectrometer, each with its specific spectral range, data acquisition, and data reduction technique, have been used. Details are not important for this study because the analysis is based on temperature differences within each individual data set, and intercomparison of absolute temperatures from different instruments is not involved. The interested reader is referred to the instrument papers listed in Table 1, and to the web link mentioned in the previous paragraph. Only for completeness, we note that the Wuppertal (WUP) data used here were obtained with spectrometer 2 described by Bittner et al. (2002), the Rikubetsu (RIK) data with the S3 spectrometer and the Sata (STA) data with the S2 spectrometer (Shiokawa et al., 2007). The instruments at ALOMAR (ALR), Oberpfaffenhofen (OPN), and Schneefernerhaus (UFS) are essentially identical to the model described in the paper by Bittner et al. (2010); the OPN instrument has now been described in much detail by Schmidt et al. (2013).

The time spans of the data that pass the selection criteria discussed below and applied consistently for all sites, and the resulting numbers of individual months (M) and nights (N) are

given in Table 2. In general, M tends to be smaller than the number of months included in the time span because of incomplete data coverage. Note that for most sites, the data sets have been acquired partly or completely before the start of NDMC. No attempt has been made to update and maximize the amount of data from each site, because it was not deemed imperative for this first multi-site study. For example, the WUP data here used are only from the more recent years, nearly completely outside the 12 years of the previous analysis by Offermann et al. (2009), with only the year 2006 included in both data sets. Consequently, the table does not give (and is not meant to give) information about the potential size of the NDMC data base, but only about the data actually used here. The data time spans vary considerably from less than one year to more than a decade, and often there is no overlap between any pair of sites. Nearly each data set (with the only exception of the recently initiated ALOMAR observations) contributed more than 20 individual months to our analysis. For some sites, more than 70 months of data were used. The number of data nights range from a few hundred to more than two thousand. Most of the data sets in Table 2 permitted a successful analysis for all of the 12 “calendar” months (i.e., the months averaged over all available years, instead of the months counted continuously throughout the data set). Obvious exceptions are the high-latitude sites during summer, when no nocturnal observations are possible.

3. Analysis technique

As in the previous studies by Offermann et al. (2006a, 2006b, 2009, 2010), we use the standard deviation of rotational temperatures as a measure of traveling PW activity. The data processing scheme was chosen after some attempts to find a reasonable compromise between sample size, data quality, and homogeneity, suitable for all the 19 different data sets. This scheme will now be described in more detail.

Before computing standard deviation, it is necessary to minimize the contribution of temporal variations outside the range of periods between 2 and about 30 days. Here we make the simplifying assumption that traveling PWs are the principal contributors to temperature variations within the 2 to 30 days period range. This is reasonable since no other mechanism of periodic variability in the mesopause region has been identified, for this period range. However, aperiodic phenomena have been

Table 2

Properties of the data sets from the sites of Table 1, and total standard deviations σ_T with statistical errors.

ID	Time span	OH temperature				O ₂ temperature			
		M	N	σ_T (K)	err(K)	M	N	σ_T (K)	err(K)
KH1	jan1991–dec2004	21	216	8.94	0.40				
ALR	dec2010–apr2011	5	116	6.80	0.41				
MAI	oct2002–apr2007	38	688	8.03	0.24				
STO	jul1991–oct1999	80	1522	8.01	0.21				
ZVE	feb2000–mar2010	93	946	5.77	0.14				
WUP	jan2006–dec2010	60	1009	5.93	0.16				
OPN	feb2009–jul2011	30	645	5.09	0.16				
UFS	jun2009–jul2011	26	492	4.66	0.17				
RIK	mar2004–may2008	37	365	7.04	0.28	37	384	6.25	0.25
DL1	jan1995–dec2001	46	257	5.15	0.22				
OSN	oct1998–nov2007	57	545	6.79	0.25	57	545	6.19	0.25
STA	dec2003–dec2010	40	394	5.90	0.24	40	393	5.88	0.20
MA1	jan2002–dec2006	52	744	5.62	0.16	52	737	6.05	0.18
CAR	feb1999–dec2001	34	264	6.39	0.28				
ALO	sep2009–may2011	21	379	6.31	0.28				
LEO	jan1998–mar2010	106	2214	5.45	0.10	106	2186	5.90	0.11
ROT	mar2002–jun2010	71	1605	8.80	0.17				
DAV	mar1997–oct2009	103	2263	5.93	0.09				
HAL	may2001–oct2009	55	1021	8.68	0.21				

observed (e.g. Scheer et al. (2005)), but they are probably too rare to contribute noticeably to the standard deviations of the present climatological study.

By basing the analysis on nocturnal means, the effect of gravity waves and tides is automatically reduced. An ad-hoc nocturnal coverage criterion of taking fully into account only nights with at least 3.5 h of data (not necessarily in a single block, but distributed over longer time spans) is meant to limit tidal contamination under unfavorable conditions. At any rate, nocturnal coverage is generally much greater than 3.5 h. This criterion also helps to make the contribution from instrumental noise negligible. However, complete tidal suppression should be impossible to obtain: In addition to variable offsets in the nocturnal means due to varying nocturnal data coverage there is also an unavoidable contribution due to the day-to-day variability of tides themselves. On the other hand, if day-to-day variations are small and nocturnal coverage is good, then tidal effects should be more or less constant and therefore contribute little to the standard deviations. We will show in Section 4.2 that there are indications in our results that tidal effects, even those due to the diurnal tide, are small.

The removal of the mean seasonal temperature variation cannot be done at all sites by subtracting the mean annual oscillations plus one or two harmonics (as done by Offermann et al. (2009)), because the inclusion of even higher harmonics might be warranted, as in the case of El Leoncito (LEO; see Reisin and Scheer (2009)). It is more practical to apply the seasonal climatology technique used by Reisin and Scheer (2009), since this can be uniformly applied for all the NDMC sites. This technique consists in defining for each day of the year (as far as possible) the center value of the 29-day running mean over the annual cycle. Of course, because of the accumulation over all the years within the time span, the 29-day window may contain much more than 29 nights.

Examples of the resulting seasonal variation of OH temperature are shown in Fig. 1 for the three midlatitude sites Delaware (DL1), Rikubetsu (RIK), and Oberpfaffenhofen (OPN). These examples are chosen because of their similar latitudes but widely spaced longitudes. Of course, the curves are not as smooth as a superposition of seasonal harmonics would be, but represent each data set as well as possible. The data sets are of small to intermediate size, but seasonal coverage is good enough to result in continuous curves for the full year. In spite of the different longitudes and time spans that belong to different years without overlap, but also the different instrumentation, the three curves have similar shapes, consistent with the typical behavior for midlatitude temperature climatologies at 87 km (see, e.g. Offermann et al. (2006b)). Any temperature offsets between the curves may be due to unavoidable systematic uncertainties of each data set, but are irrelevant

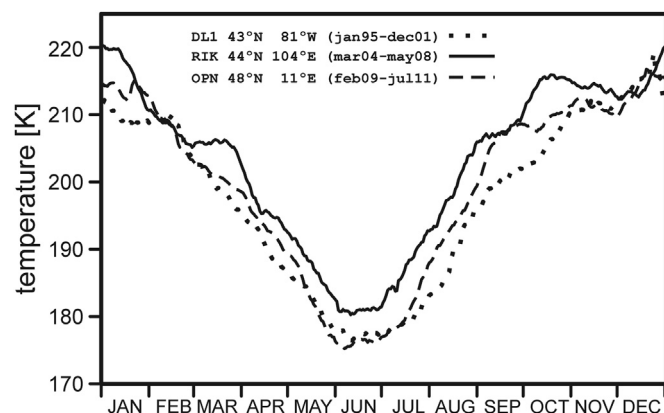


Fig. 1. Mean seasonal variation of OH temperature at Delaware (DL1), Rikubetsu (RIK), and Oberpfaffenhofen (OPN).

for the present study, since our PW analysis only uses temperature differences from any given instrument (as mentioned in Section 2).

Interannual variations can occasionally be quite strong, but are probably not related to PW power in the mesopause region (Reisin and Scheer, 2009). Therefore, artifacts from interannual variations must also be avoided. This is achieved by using $x'(d, m, y) = x(d, m, y) - \langle x \rangle(m, y)$, where d, m, y refer to the date (day, calendar month, year), $x(d, m, y)$ is the difference between the individual nocturnal means and the seasonal variation, and $\langle x \rangle(m, y)$ is the average of $x(d, m, y)$ over all days for a given individual month. As an additional quality requirement, only individual months with at least four nights (and calendar months with not less than 10 nights) are taken into account. The standard deviation for each calendar month, $\sigma(m)$, is then computed from $x'(d, m, y)$. The same procedure, but without distinguishing between months, is used to compute the standard deviation from the whole data set. This represents the mean PW activity averaged over all available calendar months, and we will call it the “total” value σ_T (which is not exactly the same as the arithmetic mean over the individual $\sigma(m)$ values).

The statistical errors of $\sigma(m)$ and σ_T cannot simply be determined by the standard formula applicable in the case of the arithmetic mean. A conceptually simple method with straightforward implementation and good performance that is equally applicable to all our data sets is the so-called jackknife. It is based, in principle, on doing the computation of (in our case) the standard deviation (as outlined above) with one data point omitted, and repeating this after omitting a different point, until all the possibilities are exhausted. The results are then combined by taking the square root of the sum-of-squares of the differences between these diminished results and the complete one (with the scale factor $(n-1)/n$, where n is the number of data; see the formula given by Efron and Gong (1983, beginning of Section 3)). The Efron and Gong paper is also an excellent exposition of the origins of this technique and its use for estimating standard error, its logical relation to the more powerful but computationally more demanding bootstrap technique, and numerical comparisons with alternative but less successful methods that were formerly considered state-of-the-art. The jackknife error so defined represents approximately the one- σ uncertainty of the final result (note that this error agrees exactly with the standard error when applied to the arithmetic mean).

We will now consider two examples to show that our PW analysis method leads to results essentially consistent with those from previous publications which used somewhat different algorithms. We compare the Wuppertal data for 2006 to 2010 obtained by the present technique with the monthly mean standard deviations for the years 1995 to 2006 as published by Offermann et al. (2009, Fig. 6), to illustrate the approximate equivalence of both approaches. As shown in Fig. 2, both variants compare favorably (the original error bars of the earlier results were standard deviations and are omitted here) for most of the months. Agreement between both data sets is excellent for 7 months (March to May, and September to December), and satisfactory for July and August. Differences appear appreciable only for January, February, and June. The enhanced PW activity of the more recent data in January and February may be related to the occurrence of major sudden stratospheric warmings (SSW) in recent years (see the review paper by Chandran et al. (2014); and references therein), but it is hard to prove for a single site (as explained in Chandran et al. (2014, p. 1286)). The total mean standard deviation σ_T from the present analysis, $5.93 (\pm 0.16)$ K (see Table 2), agrees perfectly well with the arithmetic mean of 5.99 K over the 12 monthly values by Offermann et al. (2009).

A second test is possible with data previously published for LEO, but in a different context (Reisin and Scheer, 2009). That

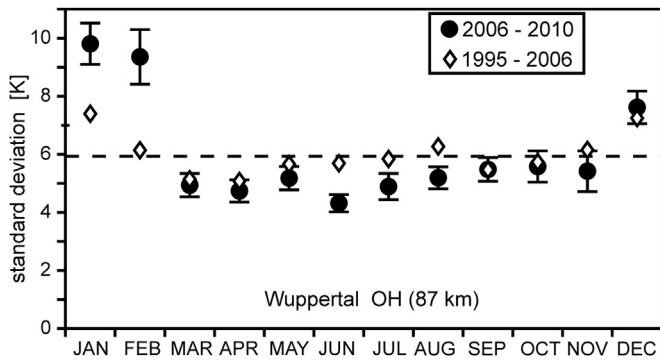


Fig. 2. Monthly standard deviations of OH temperatures at Wuppertal (WUP) obtained by Offermann et al. (2009) for the years 1995–2006 (diamonds) and the present results for 2006 to 2010 (circles). The dashed line represents the total means which practically coincide for both data sets.

paper contains yearly values of PW power between 1998 and 2007, based on a somewhat different method to the one employed now (see Fig. 8 of that paper). Since this was expressed in terms of variances, we compute the square root of the average over the yearly values, which gives 5.32 K for OH, and 5.79 K for O₂. This

can be compared with the present results of 5.45 (±0.10) K and 5.90 (±0.11) K, respectively (see Table 2), which must be considered good agreement, in view of the different arithmetic and data time spans. Again, this shows that the final results do not depend critically on the details of the analysis.

4. Results and discussion

4.1. Monthly results

The monthly standard deviations $\sigma(m)$ obtained from OH temperature measurements are shown in Fig. 3 for all the 19 sites, and are also listed in Table 3, where it is easier to appreciate the latitudinal variations (or their absence) for any given month. The $\sigma(m)$ results for the 5 sites where also O₂ temperature is measured are given in the five bottom rows of Table 3, and are plotted in Fig. 4. The larger error bars are mostly due to smaller numbers of nocturnal averages for each calendar month, although a contribution from the variability of PW activity in different years is also likely. Weather conditions inevitably play a role, and even some impact of instrumentation issues cannot be excluded. At any rate, some data sets over relatively few individual months have

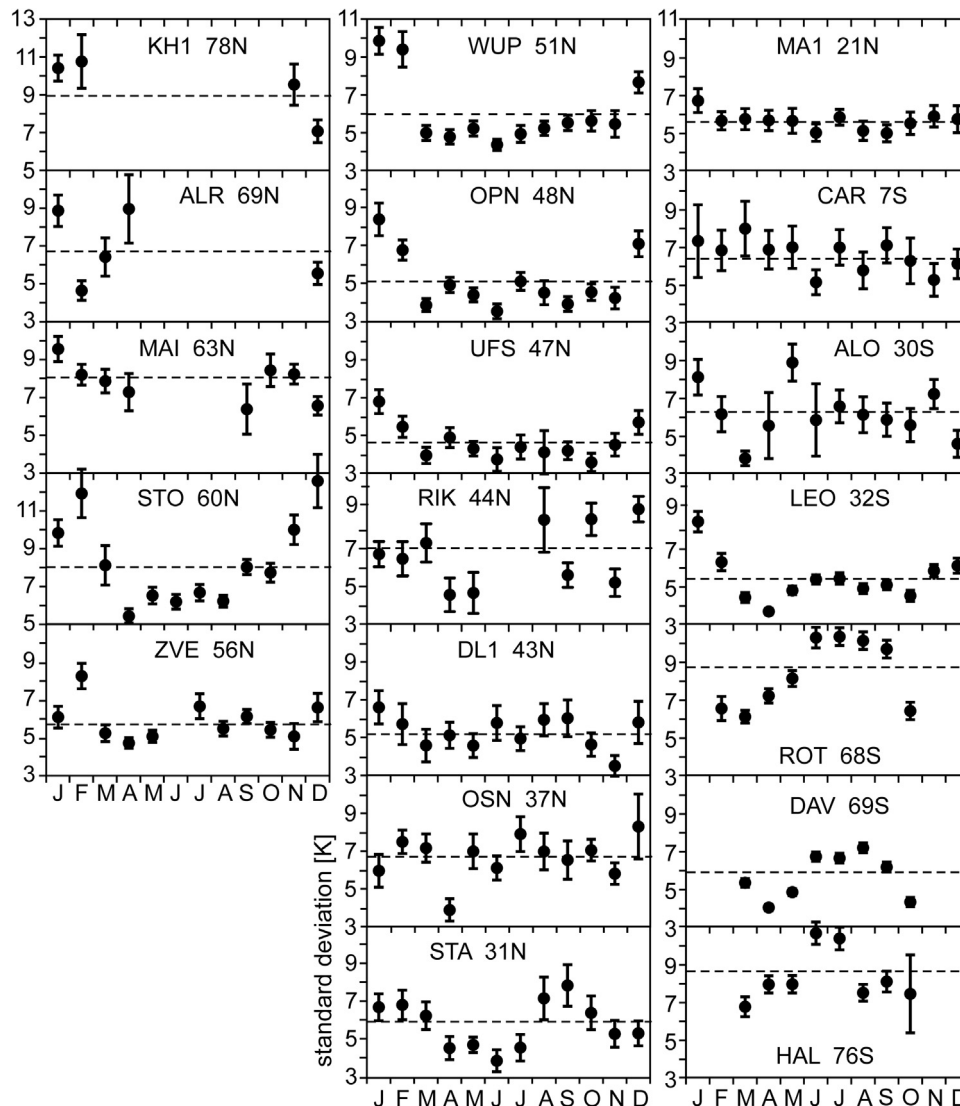


Fig. 3. Monthly values of PW activity at the 19 sites, for OH. Total values σ_T are shown as dashed lines. Sites are ordered latitudinally, columnwise, with highest northern latitude top left (as labeled). The vertical axes are in kelvins, starting at 3 K (or at 5 K for KH1 and STO).

Table 3
Monthly values of PW activity (with jackknife errors) from OH and (last five rows) O₂ data.

Site	Latitude	JAN	FEB	MAR	APR	MAY	JUN	JUL	AUG	SEP	OCT	NOV	DEC
KH1	78.15	10.4 ± 0.7	10.8 ± 1.4	–	–	–	–	–	–	–	–	9.5 ± 1.1	7.1 ± 0.6
ALR	69.28	8.9 ± 0.8	4.6 ± 0.5	6.4 ± 1.0	9.0 ± 1.8	–	–	–	–	–	–	–	5.6 ± 0.6
MAI	63.1	9.6 ± 0.7	8.2 ± 0.6	7.9 ± 0.6	7.3 ± 1.0	–	–	–	–	–	–	–	6.6 ± 0.5
STO	59.5	9.8 ± 0.7	11.9 ± 1.3	8.1 ± 1.0	5.4 ± 0.4	6.5 ± 0.4	6.2 ± 0.4	6.7 ± 0.4	6.4 ± 1.0	6.4 ± 1.3	8.4 ± 0.9	8.2 ± 0.5	12.6 ± 1.4
ZVE	55.69	6.1 ± 0.6	8.3 ± 0.7	5.2 ± 0.4	4.7 ± 0.3	5.1 ± 0.3	–	6.7 ± 0.7	5.5 ± 0.4	6.1 ± 0.4	5.4 ± 0.4	5.1 ± 0.7	6.6 ± 0.8
WUP	51.25	9.8 ± 0.7	9.4 ± 0.9	4.9 ± 0.4	4.7 ± 0.4	5.2 ± 0.4	4.3 ± 0.3	4.9 ± 0.4	5.2 ± 0.4	5.5 ± 0.4	5.6 ± 0.5	5.4 ± 0.7	7.6 ± 0.6
OPN	48.09	8.4 ± 0.9	6.8 ± 0.5	3.8 ± 0.3	4.9 ± 0.4	4.4 ± 0.4	3.5 ± 0.4	5.1 ± 0.5	4.5 ± 0.6	3.9 ± 0.4	4.5 ± 0.4	4.2 ± 0.6	7.1 ± 0.7
UFS	47.42	6.8 ± 0.6	5.5 ± 0.6	4.0 ± 0.4	4.9 ± 0.5	4.3 ± 0.4	3.7 ± 0.6	4.4 ± 0.6	4.1 ± 1.1	4.2 ± 0.5	3.6 ± 0.5	4.5 ± 0.6	5.7 ± 0.6
RIK	43.50	6.7 ± 0.7	6.5 ± 0.9	7.3 ± 1.0	4.6 ± 0.9	4.7 ± 1.1	–	–	8.5 ± 1.7	5.6 ± 0.6	8.6 ± 0.9	5.2 ± 0.7	9.1 ± 0.7
DL1	42.87	6.6 ± 0.9	5.7 ± 1.1	4.6 ± 0.9	5.1 ± 0.7	4.6 ± 0.6	5.8 ± 0.9	4.9 ± 0.6	5.9 ± 0.9	6.0 ± 1.0	4.6 ± 0.6	3.5 ± 0.5	5.8 ± 1.1
OSN	37.06	6.0 ± 0.9	7.5 ± 0.6	7.2 ± 0.8	3.9 ± 0.6	7.0 ± 0.9	6.1 ± 0.6	7.9 ± 0.9	7.0 ± 1.0	6.5 ± 1.0	7.1 ± 0.6	5.8 ± 0.6	8.3 ± 1.7
STA	31.02	6.7 ± 0.7	6.8 ± 0.8	6.2 ± 0.7	4.5 ± 0.6	4.7 ± 0.4	3.8 ± 0.6	4.5 ± 0.7	7.1 ± 1.1	7.8 ± 1.1	6.4 ± 0.9	5.3 ± 0.7	5.3 ± 0.7
MA1	20.71	6.7 ± 0.6	5.7 ± 0.5	5.8 ± 0.6	5.7 ± 0.5	5.7 ± 0.7	5.0 ± 0.5	5.9 ± 0.4	5.1 ± 0.5	5.0 ± 0.4	5.5 ± 0.6	5.9 ± 0.6	5.8 ± 0.7
CAR	–7.38	7.3 ± 1.9	6.8 ± 1.1	8.0 ± 1.5	6.9 ± 1.0	7.0 ± 1.1	5.2 ± 0.7	7.0 ± 0.9	5.8 ± 1.0	7.1 ± 0.9	6.3 ± 1.2	5.3 ± 0.9	6.1 ± 0.8
ALO	–30.25	8.1 ± 0.9	6.2 ± 0.9	3.8 ± 0.4	5.6 ± 1.7	8.9 ± 1.9	5.9 ± 1.9	6.6 ± 0.9	6.1 ± 0.9	5.9 ± 0.9	5.6 ± 0.9	7.2 ± 0.8	4.6 ± 0.7
LEO	–31.80	8.5 ± 0.5	6.3 ± 0.5	4.4 ± 0.3	3.7 ± 0.2	4.8 ± 0.2	5.4 ± 0.2	5.4 ± 0.3	4.9 ± 0.3	5.1 ± 0.3	4.5 ± 0.3	5.9 ± 0.3	6.1 ± 0.4
ROT	–67.57	–	6.6 ± 0.6	6.1 ± 0.3	7.2 ± 0.4	8.1 ± 0.4	10.3 ± 0.5	10.4 ± 0.5	10.1 ± 0.5	9.7 ± 0.5	6.4 ± 0.5	–	–
DAV	–68.58	–	–	5.4 ± 0.2	4.1 ± 0.2	4.9 ± 0.2	6.8 ± 0.3	6.7 ± 0.3	7.2 ± 0.3	6.2 ± 0.3	4.4 ± 0.3	–	–
HAL	–75.52	–	–	6.8 ± 0.5	8.0 ± 0.4	8.0 ± 0.5	10.7 ± 0.6	10.4 ± 0.6	7.6 ± 0.4	8.1 ± 0.6	7.5 ± 2.1	–	–
RIK	43.50	8.4 ± 0.7	6.4 ± 0.8	5.6 ± 0.7	5.8 ± 0.9	7.6 ± 1.7	–	–	5.2 ± 0.9	5.3 ± 0.9	5.7 ± 0.8	4.3 ± 0.5	6.7 ± 0.7
OSN	37.06	5.3 ± 1.0	6.5 ± 0.6	5.0 ± 0.4	5.8 ± 0.9	5.8 ± 1.0	5.1 ± 0.6	7.5 ± 1.0	6.6 ± 0.7	5.6 ± 0.5	5.9 ± 0.8	7.0 ± 0.6	8.3 ± 2.1
STA	31.02	7.1 ± 0.9	5.5 ± 0.6	6.7 ± 0.8	6.0 ± 0.8	6.6 ± 0.8	4.9 ± 0.9	5.6 ± 0.8	5.6 ± 0.7	6.1 ± 0.8	6.5 ± 0.9	5.9 ± 0.6	5.0 ± 0.4
MA1	20.71	5.1 ± 0.7	7.5 ± 1.0	6.7 ± 0.5	5.7 ± 0.6	5.8 ± 0.6	4.6 ± 0.4	5.8 ± 0.5	5.5 ± 0.5	6.9 ± 0.6	6.3 ± 0.5	6.2 ± 0.4	5.9 ± 0.5
LEO	–31.80	8.1 ± 0.5	5.8 ± 0.4	5.0 ± 0.4	4.8 ± 0.3	6.0 ± 0.3	6.1 ± 0.3	6.1 ± 0.4	5.9 ± 0.4	6.4 ± 0.4	5.4 ± 0.3	5.8 ± 0.4	5.3 ± 0.3

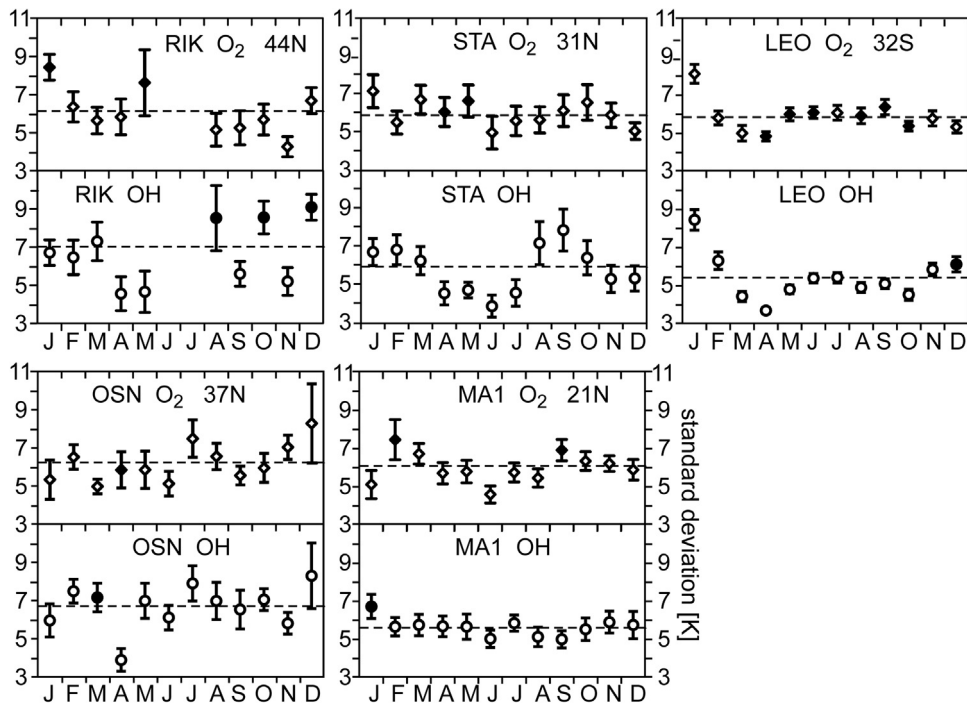


Fig. 4. Monthly values of PW activity at sites which also measure O₂ temperature (shown as diamonds). Results derived from OH (circles) are the same as in Fig. 3. Filled symbols are used for data where activity is significantly higher than at the other emission height. Units, scale, and organization as in Fig. 3.

reasonably small error bars. Note that Figs. 3 and 4 also show total activity σ_T for each site, to guide the eye (dashed lines; σ_T is further discussed in Section 4.2).

The variation of monthly PW activity values from OH data (Fig. 3) ranges from rather constant (for Maui, MA1) to strong seasonal modulation (for Stockholm, STO and Rothera, ROT). Fairly quiet behavior (with small deviations from σ_T), although not as constant as MA1, is exhibited in Cariri (CAR), but also, with slightly more variation, at DL1. So, we find the lowest month-to-month variation at the two tropical sites (MA1 at 21° N, and CAR at 7° S).

Some sites, while rather quiet for most of the year, show a tendency for higher PW activity from December to February. This is the case for UFS, WUP, OPN, Zvenigorod (ZVE), and LEO. These sites are from northern midlatitudes between 47° N (UFS) and 56° N (ZVE), but surprisingly also include the southern midlatitude site LEO (32° S). The variability of PW activity at RIK (44° N), Sierra Nevada (OSN; 37° N), and STA (31° N) is somewhat stronger than at the other midlatitude sites.

Although not so obvious from Fig. 3, the variations of $\sigma(m)$ at LEO and the nearby station Cerro Pachón (ALO at 30° S; 220 km

from LEO) are similar for most of the year. Ten months are in fact consistent within combined error bars (see Table 3). The greatest discrepancy is the high value at ALO in May. This is probably due to poor tidal reduction for this month in which the tidal activity is known to be strong. We conclude this, because improving tidal suppression by changing the nocturnal coverage criterion from 3.5 h to 5.8 h decreases the ALO value for May from $8.9 (\pm 1.0)$ K to $6.7 (\pm 1.1)$ K, which is much closer to the corresponding value at LEO.

Among the three Antarctic sites Rothera (ROT; 68° S), Davis (DAV; 69° S), and Halley (HAL; 76° S), the seasonal patterns are similar, with higher PW activity in winter and lower activity in late autumn and early spring (as far as night conditions at those latitudes permit measurements). Such smooth transitions from month to month as at ROT and DAV have not been documented with similar quality at the northern high latitude sites Longyearbyen (KH1; 78° N), ALR (69° N), and Maimaga (MAI; 63° N). This smoothness in Antarctica may be a consequence of the absence of major SSW events in the Southern Hemisphere (except in 2002). The much greater amount of usable data reflecting more favorable Antarctic weather conditions may also play a role.

The increased PW activity at northern high latitudes in January and February may be related to major SSW events, which occur irregularly in about one half of the winters (see Chandran et al. (2014, Table 1)), but, as mentioned, are expected to perturb temperature at different sites in a different way. The low PW activity in February over ALR (see Fig. 3) may be due (at least, in part) to the absence of major and minor SSWs in the 2010–2011 winter (Chandran et al., 2014), the only one contributing to the ALR data.

With respect to the results derived from O_2 temperatures, the month-to-month variability of PW activity is rather small at Maui (MA1), LEO, STA, and OSN (see Fig. 4), and moderately strong at RIK. This is not inconsistent with the behavior of the OH results in this limited latitudinal range between 44° N and 32° S.

These five sites where OH and O_2 temperatures are available permit comparison of PW activity at the nominal altitudes of 87 and 95 km. The strongest correlation between the month-to-month variations of $\sigma(m)$ at both altitudes is evident at LEO, already from visual inspection of Fig. 4. The correlation coefficient is 0.82. Before we can tell whether this number really signals a strong similarity, we must determine its uncertainty (which is unfortunately rarely done in the literature). We can do this easily with the jackknife, which results in a one- σ error of ± 0.35 (let us ignore that the upper limit exceeds somewhat the maximum

possible correlation of 1, which is not an inherent fault of the jackknife; the excess becomes smaller when the correlation coefficient approaches ± 1). So, the correlation is definitely positive.

The low seasonal variability of $\sigma(m)$ at MA1 at both altitudes (as mentioned above; also see Fig. 4) signals a similar behavior of PW activity. However, the approximately constant PW activity cannot be adequately dealt with by the correlation coefficient (which is -0.09 ± 0.50 , formally consistent with no correlation at all, but practically meaningless).

According to Fig. 4, there is a certain similarity between both altitudes at STA, as well as at OSN. This impression is confirmed by the correlation coefficients of 0.34 ± 0.27 and 0.48 ± 0.27 , respectively. Here, these numbers make sense, because of the non-vanishing variability in the parameters involved. For RIK, the correlation coefficient -0.01 ± 0.33 is consistent with zero, similarly to the result for Maui, but here it reflects the relatively irregular seasonal pattern, especially for the OH data. A relation of this irregularity to difficult weather conditions is not obvious, but cannot be completely ruled out (weather conditions did cause insufficient data coverage for our analysis in June and July). So, we can say that the results (except for RIK) support the conclusion that seasonal variations of PW activity at both altitudes of observation are similar.

PW activity at the two altitudes is consistent within combined error bars (see Table 3) for most (67%) of the 58 pairs of monthly values documented at these five sites, while there is more activity at 95 km for 22%, or at 87 km for only 10%, of the cases. No seasonal preference is evident for the cases where PW activity changes with altitude (as shown clearly by the filled symbols in Fig. 4 which signal the emission layer with higher activity).

4.2. Total wave activity

The total values of PW activity σ_T for each site and both emissions vary between $4.66 (\pm 0.17)$ K and $8.94 (\pm 0.4)$ K (see Table 2). The median is 6.12 K, and one half of the data fall in the narrow range from 5.6 to 6.4 K, including all the values for O_2 . For the sites where both emissions are observed, there is almost no difference on average between the total PW activity at the two altitudes, and a maximum difference of only about 0.8 K (see Table 2). This similarity seems to confirm the absence of a persistent mesospheric surf zone close to the mesopause region. As shown by, e.g., Sassi et al. (2002), the mesospheric surf zone is only a temporary, mostly winter time, feature. Our monthly results contain no evidence of any winter preference, as mentioned (at the end of the previous section).

To more easily appreciate how PW activity varies with latitude, we plot σ_T versus latitude (see Fig. 5). Indeed, many results from DAV at 69° S to ALR at 69° N are in, or close to, the narrow range mentioned (hatched area in Fig. 5). However, this does not exclude the possibility of any latitudinal effect, because all the other high-latitude sites (HAL, ROT, STO, MAI, KH1) have significantly higher PW activity of about 8 K, or more. Only some part of these high values may be related to missing summer data, but not at STO, where summer is especially well covered. One can also imagine a contribution from quasi-stationary PWs that would be strongest at sites which happen to be close to the nodes of the wave pattern. There, spatial shifts of quasi-stationary PWs would be observed as temporal variations and so confounded with traveling PWs. This effect might explain at least part of the discrepancies among the high-latitude sites.

There are also data somewhat outside the narrow range that belong to midlatitude sites. Year-to-year variations of PW activity (e.g., as discussed by McDonald et al. (2011), for the 16-day wave) could explain differences in σ_T values for sites of similar latitude but with different data time spans.

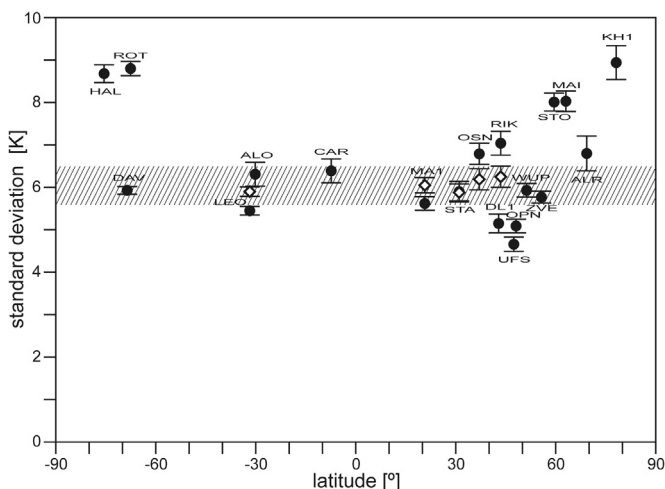


Fig. 5. Latitudinal distribution of total planetary wave activity σ_T , for OH (circles) and O_2 rotational temperatures (diamonds). Narrow range covered by 50% of the data points is shown as hatched area.

This may be why the value for UFS, based on little more than two years of data, is relatively small. The same argument should also hold for OPN, only 80 km away (although the separation between the respective fields of view is about twice as large), where the data set covers the UFS time span, but starts four months earlier. If the four additional months are excluded from the analysis, OPN and UFS agree within the combined error bars, so that no contradiction is left.

Although the observed latitudinal pattern of PW activity cannot be described schematically in a single way, we can identify two extreme, simplified views of these results: We may regard the total values of PW activity as approximately constant for all latitudes (“scenario 1”), or assume that this constant value (6.12 K) only applies to low and middle latitudes, but that wave power slopes upwards, at high latitudes (“scenario 2”). Therefore, at latitudes higher than approximately $\pm 40^\circ$, both scenarios become more and more incompatible, that is, contradictory in that they do not do justice to all the data. Both scenarios should be replaced by a unified representation, but this is outside the scope of our present study and would probably require the inclusion of atmospheric modeling. At any rate, the absence of variation at low and middle latitudes may be taken as indirect evidence that tidal contamination of our data is indeed small. In theory, the diurnal tide has the greatest potential of aliasing into the PW activity results. This tide would lead to a latitudinal modulation because of its dominance in the equatorial region (e.g., Achatz et al. (2008) and Shepherd et al. (2012)), but this is not what we observe. We will return to the two simplified scenarios in the next section.

No special feature of the σ_T variation as a function of longitude can be distinguished and Fig. 6 shows no sign of a longitudinal dependence. This is also evident from the fact that the full range of σ_T is covered by the 6 values in the narrow longitude range from 7° E to 18° E (UFS, OPN, WUP, ALR, STO, and KH1; all being northern mid- and high-latitude sites). The absence of a longitudinal dependence is to be expected for traveling PWs.

4.3. SABER proxy validation

As mentioned in the introduction, Offermann et al. (2009) have defined a SABER traveling PW activity proxy for the latitudes of 20° N, 50° N, and 70° N. At 50° N, this proxy has already been successfully tested in that paper using the very long Wuppertal OH data set. Therefore, our present results for WUP, while being

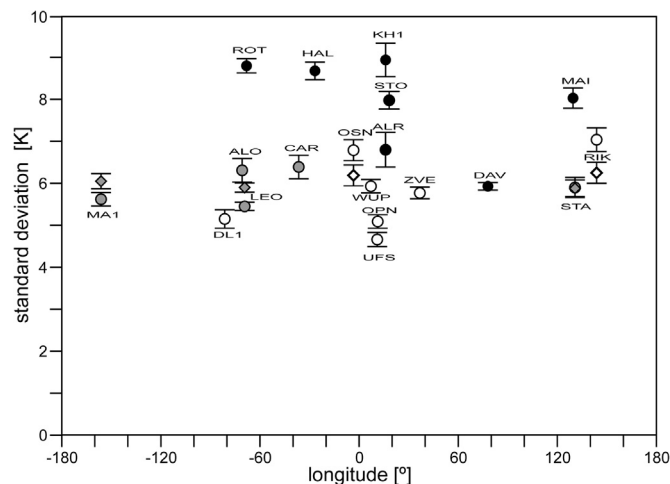


Fig. 6. Longitudinal distribution of total planetary wave activity σ_T , for OH (circles) and O_2 rotational temperatures (diamonds). Different filling styles are used to distinguish sites at high latitude (black), midlatitude (white), and low latitude (gray).

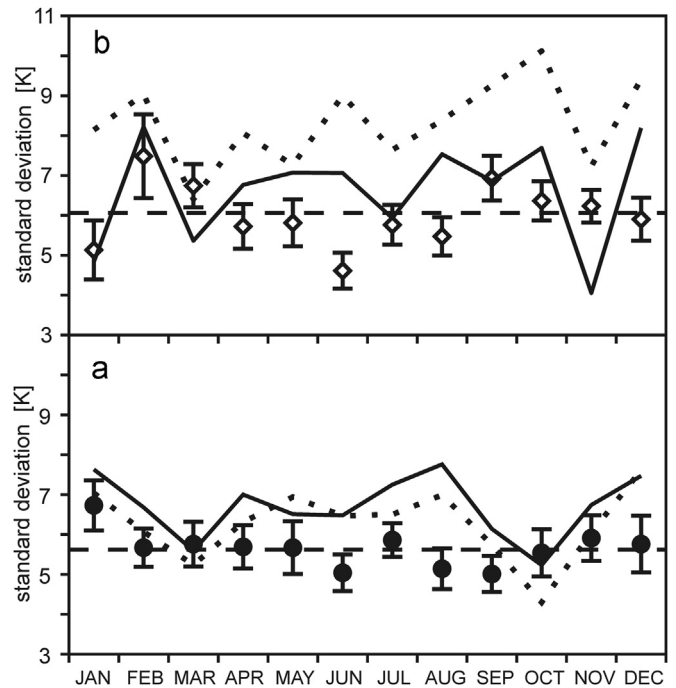


Fig. 7. Monthly values of PW activity at Maui for OH (panel a, circles) and O_2 (panel b, diamonds) compared to results deduced from SABER data at 20° N (Offermann et al., 2009) for 86 and 88 km (solid and dotted lines, respectively; panel a), and for 94 and 96 km (solid and dotted lines; panel b). Total averages for Maui are shown by horizontal dashed lines.

essentially consistent with the Offermann et al. (2009) analysis, cannot improve upon that test.

Our results for Maui (MA1) are useful to extend the test of the SABER proxy to 20° N (Offermann et al. (2009, Table 1)), not only for the OH layer, but also for the O_2 layer. The time span for MA1 agrees pretty well with the years which define the SABER proxy, so that interannual variations should have little impact. The results for MA1, and the SABER proxy for the two altitudes closest to each nominal emission height (i.e., 86, 88, 94, and 96 km) are shown in Fig. 7, which also gives an impression of the uncertainties involved. In general, the proxy is slightly greater than the Maui OH data (by about 0.9 K, on average; panel a), but in view of the complexity of the proxy scheme, this still may be interpreted as good agreement. For the O_2 layer (panel b), the proxy at 94 km is only about 0.7 K higher than the airglow data, which means that the agreement is also good. However, the performance of the proxy is noticeably poorer at 96 km (about 2.3 K greater than the O_2 result). It is hard to tell what could cause such a relatively strong difference in the behavior of the proxy at these two consecutive height levels only 2 km apart. Notwithstanding, we can conclude from this test that the SABER proxy performs well at 20° N, for the OH airglow emission height, and also at 94 km.

For a comparison at 70° N, the only available site is ALOMAR (ALR). Even though the ALR data only cover a few individual months, a preliminary test of the SABER proxy can already be done. Since two months, for which ALR results are available, are not covered by the proxy at this latitude, only January to March can be used. The ALR values for these months are $8.9 (\pm 0.8)$ K, $4.6 (\pm 0.5)$ K, and $6.4 (\pm 1.0)$ K, while the corresponding SABER proxies are 5.9 K, 7.3 K, and 5.8 K (derived via the mean variance from the standard deviations at 86 and 88 km by Offermann et al. (2009, Table 1)). In spite of the differences for each of the three months, a compensating effect of opposite signs leads to a rather small total discrepancy between the proxy and the ALR results. The total mean proxy is only $0.32 (\pm 0.51)$ K greater than the ALR

value. The error bar, which mainly stems from the jackknife errors from ALR, probably underestimates the true uncertainty because of the short time span and lack of overlap with the SABER data base. At any rate, in view of the limited information available in this case, the comparison may be judged satisfactory.

4.4. SCIAMACHY OH temperatures

By combining the total PW activity presented so far with the activity of planetary and other waves derived from satellite-based OH rotational temperature data, we can obtain other useful information about wave dynamics in the mesopause region. Such data are available from the SCIAMACHY instrument, a spectrometer on the ESA environmental satellite Envisat (Burrows et al., 1995; Bovensmann et al., 1999; von Savigny et al., 2004, 2012b). The limb scan data set used here covers the time span from August 2002 to December 2009 and is divided into latitudinal zones 10° wide, centered on the latitudes from −30° to +70°. Our analysis is based on the variances of the *N* daily means for each zone, but not on the daily means themselves. These daily variances essentially represent the geophysical contributions from planetary (traveling and stationary) and gravity waves, but also include the mean statistical error of the individual measurements (“noise”). Because of the sun-synchronous orbit, migrating tides are expected to contribute very little to these daily variances. The numbers *N* (see Table 4) of daily values (which are only based on observations at a nearly constant local night time, during 24 UT hours) are greater than 1000 (except at 70° N), and so comparable with the upper range of *N* for the ground-based data (Table 2).

By averaging the daily variances, the corresponding total standard deviations for each zone are obtained (see 3rd column in Table 4 and small circles connected by straight lines in Fig. 8; the errors are determined by the jackknife). Note that by design, the mean seasonal and interannual temperature variations do not affect these results, in contrast to the ground-based data where both effects had to be removed explicitly. On the other hand, these results still contain an unspecified amount of noise, to be estimated below. We assume that the instrument noise is constant, not depending on latitude or longitude. This is a reasonable assumption if latitudinal differences of airglow brightness are ignored. The latitudinal variation of the SCIAMACHY results should only be due to differences in wave activity.

The SCIAMACHY wave activity peaks at the equator. We have tested the possibility of artifacts from electronic perturbations in the South Atlantic Anomaly (SAA) region to affect these results. This test consisted in analyzing a subset of the data, where the longitude range between 80° W and 30° E was excluded. Since the main features did not change, it is reasonable to discard any major impact of SAA artifacts on the present results.

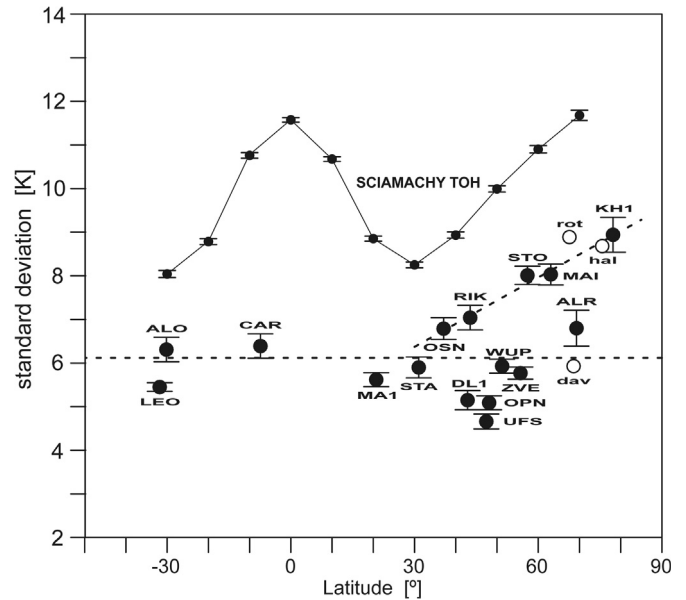


Fig. 8. Latitudinal distribution of the activity of different waves and noise from SCIAMACHY OH rotational temperatures (small circles connected by straight lines), and also of ground station σ_T for OH (big circles). The two dashed lines show the median value for all ground stations, and a linear fit through the points for STO, MAI and KH1. For comparison, data from southern high latitudes (ROT, DAV, HAL) are mirrored north (open circles and lower case IDs).

The SCIAMACHY wave activity shows a good interhemispheric symmetry at all latitudes where data from both hemispheres are available (i.e., from −30° to +30°), and then rises monotonically at higher northern latitudes (Fig. 8). Each value is greater than all the ground-based data in the same latitude zone. This is consistent with the expectation that the SCIAMACHY data include the effect of other wave types in addition to traveling PWs and instrument noise. This additional contribution is simply the difference between the satellite and ground-based variances. As mentioned in Section 4.2, the ground-based variances can be represented by two alternative scenarios, which we can now take advantage of. In scenario 1, the traveling PW activity is independent of latitude with a constant standard deviation of 6.12 K and the additional contribution is expressed as standard deviation or variance under the $\Delta 1$ header of Table 4.

Scenario 2, supported by some high latitude sites, may be quantified by a linear fit through the standard deviations for STO, MAI, and KH1, as shown by the sloping dashed line in Fig. 8. It turns out that this line is also fairly consistent with data for OSN and RIK, and also with the Antarctic stations ROT and HAL “mirrored” to the Northern Hemisphere. But as mentioned, DAV

Table 4
Wave activity results obtained from SCIAMACHY OH temperatures (see text for details).

Latit.	<i>N</i>	SCIAMACHY	$\Delta 1$		$\Delta 2$		$\Delta 3$
		std (K)	std (K)	var(K ²)	std (K)	var(K ²)	std (K)
30° S	1039	8.04 ± 0.08	5.21	27.2			2.26
20° S	1358	8.78 ± 0.07	6.30	39.7			4.20
10° S	1621	10.76 ± 0.06	8.85	78.3			7.50
0°	2225	11.58 ± 0.05	9.82	96.5			8.63
10° N	2361	10.68 ± 0.05	8.75	76.5			7.38
20° N	2307	8.85 ± 0.06	6.39	40.9			4.34
30° N	1951	8.25 ± 0.07	5.53	30.6			2.92
40° N	1507	8.93 ± 0.07	6.51	42.3	5.67	32.2	3.18
50° N	1329	9.99 ± 0.07	7.90	62.4	6.68	44.6	4.74
60° N	1002	10.90 ± 0.08	9.02	81.4	7.44	55.4	5.77
70° N	635	11.68 ± 0.12	9.95	98.9	8.02	64.3	6.50

conforms much more closely to scenario 1, as do the other sites at more than 40° N (DL1, UFS, OPN, WUP, ZVE, ALR). Using this fit, we obtain smaller values for this additional contribution at 40° N to 70° N ($\Delta 2$ of Table 4). For latitudes farther south, $\Delta 2$ is equal to $\Delta 1$.

As mentioned, $\Delta 1$ and $\Delta 2$ describe a superposition of gravity waves, stationary PWs, and noise (and perhaps a contribution from nonmigrating tides and tidal variability). For 30° S, this mixture can be disentangled in part, by using published results on gravity wave activity at LEO (Reisin and Scheer, 2004). Those results were based on data from 1998 to 2002 and are free from the contribution of tides and LEO photon counting noise. By averaging over the seasonal variation of gravity wave variance for OH temperature given in Fig. 4d of that paper, a total gravity wave variance at LEO of $12.3 (\pm 0.14) \text{ K}^2$ is obtained. Because of the differences in ground-based (zenith) and satellite (limb) viewing geometry, the small horizontal wavelengths involved, and other observational constraints, the LEO gravity wave activity and the zonal mean observed by SCIAMACHY need not agree, so that the LEO result can only be regarded as a proxy for SCIAMACHY gravity wave activity.

The standard deviation for traveling PWs at LEO (σ_T of Table 2) corresponds to the variance of $29.7 (\pm 1.1) \text{ K}^2$, while the total variance for SCIAMACHY at 30° S is $64.0 (\pm 1.1) \text{ K}^2$. Subtracting from the SCIAMACHY value the LEO contributions for gravity and traveling planetary wave activity, we obtain $22.0 (\pm 1.6) \text{ K}^2$ as the combination of data noise and maybe stationary PWs. Note that the resulting standard deviation, 4.7 K, is somewhat smaller than previous estimates of retrieval error for an individual measurement (von Savigny et al., 2004), so that this number may also be regarded as an improved upper limit of mean SCIAMACHY OH temperature noise. This number is probably quite realistic, since stationary PWs at low latitude are negligibly weak, in comparison (see Offermann et al. (2009, Fig. 8b)). In what follows, we take the value of 22.0 K^2 as the SCIAMACHY noise variance for all latitudes.

With these ingredients so defined, we can estimate the latitudinal distribution of the activity of a combination of waves (gravity waves, stationary PWs, and possibly, tidal residuals, but excluding traveling PWs and noise), under scenario 2 for traveling PWs. The corresponding variance is $\Delta 2$ minus 22.0 K^2 . The standard deviations are given in column $\Delta 3$ of Table 4, and are plotted as circles in Fig. 9. Of course, the interhemispheric symmetry at low latitudes is unaffected by the subtraction of

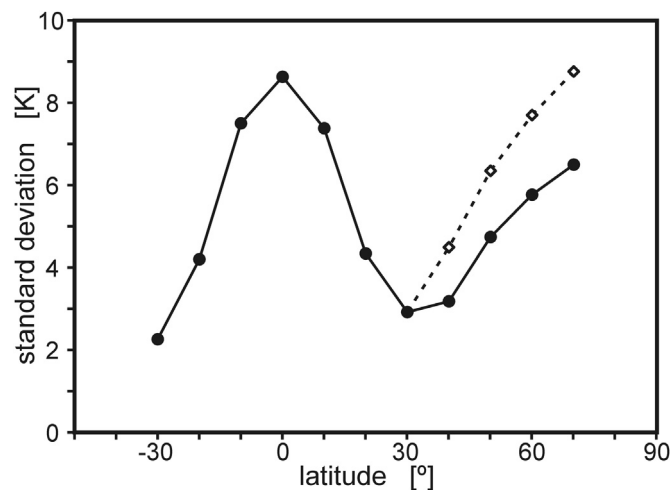


Fig. 9. Latitudinal distribution of SCIAMACHY wave activity excluding traveling planetary waves via constant activity scenario (diamonds connected by dashed lines), or via scenario 2 (from column $\Delta 3$ of Table 4; circles connected by straight lines). Both scenarios agree from 30° S to 30° N.

constant terms. At higher latitudes, the assumed rise in traveling PW activity of scenario 2 is not strong enough to remove the monotonic growth of other wave types. The consequences of the constant traveling PW scenario 1 are shown as diamonds connected by dashed lines, in Fig. 9. The true behavior at 40° N to 70° N is probably intermediate between the results from both scenarios.

The question of which waves are responsible for the shape of the figure, can be separated into two parts: First, which wave type causes this massive concentration of variance over the equator (about four times the wave power at $\pm 20^\circ$, and 10 times the power at $\pm 30^\circ$)? Second, which wave type is mainly responsible for the increase at higher northern latitudes? Both questions may have different answers. As far as we can tell from the present evidence, gravity waves, stationary PWs, nonmigrating tides may be involved, but their relative proportions are not clear. Our second question has a plausible answer, in that stationary PWs are probably the main contribution at higher latitudes. In this context one has to keep in mind that the SCIAMACHY high latitude observations are only performed during the winter months, where stationary PW activity is expected to be larger than during the summer months, because of the Charney–Drazin criterion. The increase in standard deviation with increasing northern latitude seen in Fig. 9 is therefore affected by the transition from all-year coverage at low latitudes to winter-only coverage at high latitudes. The stationary PW study by Mukhtarov et al. (2010) based on 6 years of SABER data between 50° S and 50° N shows a similar monotonic increase in activity with latitude, which seems to be even quantitatively consistent with our Fig. 9 (and column $\Delta 3$ of Table 4). However, stationary PW activity is practically absent at the equator (Mukhtarov et al., 2010). On the other hand, while it is known that nonmigrating tides do maximize at the equator, they may be too weak to account for the observed equatorial activity (see, e.g., Achatz et al. (2008)). Therefore, it is reasonable to assume that the equatorial maximum is caused by gravity waves, although there is presently no other confirming evidence for the mesopause region, except maybe the findings about the association between gravity waves and the diurnal tide from perturbed WINDII airglow emission profiles by Liu and Shepherd (2006).

5. Summary and conclusions

The analysis of rotational temperature time series from 19 NDMC sites at latitudes between 78° N and 76° S has resulted in 19 monthly climatologies of traveling planetary wave power at the nominal altitude of 87 km, and also in 5 climatologies at 95 km, which lead to the following findings.

1. There is little variation of the monthly values at the two tropical sites (at 7° S and 20° N).
2. There is only moderate variation for most of the year, but eventually more elevated activity from December to February at seven of the 10 midlatitude sites (of both hemispheres, namely between 32° S to 56° N).
3. The strongest variations occur at all the seven high latitude sites (at 76° S to 68° S, and from 60° N to 78° N).
4. From sites where data from both altitudes are available, we conclude that the variation of monthly values, but also the total mean activity levels (i.e., averaged over all available months) at 87 km and 95 km are similar.
5. These total mean traveling planetary wave activity values (expressed as standard deviations) for all the sites fall into two distinct groups: most sites exhibit activity levels concentrated around 6 K (including sites at 69° S and 69° N), while five high latitude sites show considerably higher activity of 8 to 9 K.

6. Consistent with the behavior of traveling planetary waves, there is no evidence for a variation of wave activity with longitude.
7. Our interpretation of data from two sites permits to extend the test of the SABER proxy for the traveling planetary wave climatology by Offermann et al. (2009). At 20° N, the proxy is confirmed for the altitudes of 87 km and 94 km, while at 70° N, more limited evidence supports the proxy for 87 km.
8. The present results on traveling planetary waves were also used to derive the latitudinal variation of the activity of other wave types by using SCIAMACHY OH temperature fluctuations at latitudes between 30° S and 70° N. We find a pronounced equatorial maximum, so narrow that wave power drops to one half at only $\pm 15^\circ$ latitude, and additionally, a monotonic wave activity increase from 40° N to 70° N. There are reasons to attribute the equatorial maximum mainly to gravity waves. On the other hand, the paper by Mukhtarov et al. (2010) contains evidence which suggests that the rise towards high northern latitudes may be essentially due to stationary planetary waves.

We are not aware of any theoretical prediction of the net power of traveling planetary waves for the mesopause region, though some models might be able to produce such a prediction, in future. The present study is an outcome of the NDMC Thematic Area “Planetary Waves”. Presently, NDMC comprises airglow instruments at approximately 50 sites world-wide, which is more than twice the number of sites involved here. Furthermore, data acquisition at most sites is actively pursued, so we may expect continuing high scientific productivity from NDMC. A growing temporal and global coverage of the available data base will permit more detailed studies in the future.

Acknowledgments

We thank Marianna Shepherd and Alok Taori for supplying data from Eureka and Gadanki, which regrettably were still insufficient to pass the selection criteria and so yielded no usable results. Helpful comments by Dirk Offermann and by the anonymous reviewers of previous manuscript versions are gratefully acknowledged. E.R.R. and J.Sch. acknowledge funding by CONICET, Argentina Grant PIP 112-200801-00287. M.E.D and F.S. would like to acknowledge financial support from the Research Council of Norway (RCN) through the projects: High-Arctic Gravity waves and their impact on middle atmospheric circulation and temperature (#204993), and Norwegian and Russian Upper Atmosphere Cooperation On Svalbard part 2 # 196173/S30 (NORUSCA2). C.S.D. acknowledges support to the Geophysical Institute by Atmospheric Sciences Division of the US National Science Foundation. V.I.P. and A.I.S. are grateful to RFBR for support of the airglow observations at Zvenigorod station. M.J.L.G. and E.R. acknowledge funding by the Spanish MICINN under Project AYA2011-23552 and thank the staff of Sierra Nevada Observatory for assistance with the SATI instrument. K.S. thanks M. Satoh, Y. Katoh, Y. Hamaguchi, and Y. Yamamoto of STEL, Nagoya Univ., for their helpful support of the photometer operation at RIK and STA, and acknowledges support by Grant-in-Aid for Scientific Research (11440145, 13573006) and by Priority Area-764 (13136201) of MEXT, Japan. Financial support for the MTM observations and data analysis as part of the Maui-MALT program and Cerro Pachon Program was provided by NSF Grants ATM-03-38425, ATM-0003218 and ATM-1110215. Observations at Davis are supported by the Australian Antarctic Science Advisory Committee (ASAC) under AAS701 and we thank the Davis wintering science teams for their dedicated observatory support. SCIAMACHY is jointly funded by Germany, the Netherlands, and

Belgium. The analysis of SCIAMACHY data is supported by the Universities of Bremen and Greifswald, and the SCIAMACHY Level 1 data were kindly provided by ESA.

References

- Achatz, U., Grieger, N., Schmidt, H., 2008. Mechanisms controlling the diurnal solar tide: Analysis using a GCM and a linear model. *J. Geophys. Res.* 113 (A8), A08303, <http://dx.doi.org/10.1029/2007JA012967>.
- Ammosov, P.P., Gavril'yeva, G.A., 2000. Infrared digital spectrograph for hydroxyl rotational temperature measurements. *Instrum. Exp. Tech.* 43, 792–797. (translated from *Pribory i tekhnika eksperimenta*).
- Bittner, M., Offermann, D., Graef, H.H., 2000. Mesopause temperature variability above a midlatitude station in Europe. *J. Geophys. Res.* 105 (D2), 2045–2058.
- Bittner, M., Offermann, D., Graef, H.-H., Donner, M., Hamilton, K., 2002. An 18-year time series of OH rotational temperatures and middle atmosphere decadal variations. *J. Atmos. Sol.-Terr. Phys.* 64 (8–11), 1147–1166.
- Bittner, M., Höppner, K., Pilger, C., Schmidt, C., 2010. Mesopause temperature perturbations caused by infrasonic waves as a potential indicator for the detection of tsunamis and other geo-hazards. *Nat. Hazards Earth Syst. Sci.* 10, 1431–1442.
- Bovensmann, H., Burrows, J.P., Buchwitz, M., Frerick, J., Noël, S., Rozanov, V.V., Chance, K.V., Goede, A.P.H., 1999. SCIAMACHY: mission objectives and measurement modes. *J. Atmos. Sci.* 56 (2), 127–150.
- Buriti, R.A., Takahashi, H., Gobbi, D., de Medeiros, A.F., Nepomuceno, A.A., Lima, L. M., 2004. Semiannual oscillation of the mesospheric airglow at 74° S during the PSMOS observation period of 1998–2001. *J. Atmos. Sol.-Terr. Phys.* 66 (6–9), 567–572.
- Buriti, R.A., Takahashi, H., Lima, L.M., Medeiros, A.F., 2005. Equatorial planetary waves in the mesosphere observed by airglow periodic oscillations. *Adv. Space Res.* 35, 2031–2036.
- Burrows, J.P., Hölzle, E., Goede, A.P.H., Visser, H., Fricke, W., 1995. SCIAMACHY – scanning imaging absorption spectrometer for atmospheric cartography. *Acta Astronaut.* 35 (7), 445–451.
- Chandran, A., Collins, R.L., Harvey, V.L., 2014. Stratosphere–mesosphere coupling during stratospheric sudden warming events. *Adv. Space Res.* 53, 1265–1289.
- Efron, B., Gong, G., 1983. A leisurely look at the bootstrap, the jackknife, and cross-validation. *Am. Stat.* 37 (1), 36–48.
- Espy, P.J., Stegman, J., 2002. Trends and variability of mesospheric temperature at high-latitudes. *Phys. Chem. Earth* 27, 543–553.
- Espy, P.J., Stegman, J., Witt, G., 1997. Interannual variations of the quasi-16-day oscillation in the polar summer mesospheric temperature. *J. Geophys. Res.* 102, 1983–1990.
- Espy, P.J., Hibbins, R.E., Jones, G.O.L., Riggan, D.M., Fritts, D.C., 2003. Rapid, large-scale temperature changes in the polar mesosphere and their relationship to meridional flows. *Geophys. Res. Lett.* 30 (5), <http://dx.doi.org/10.1029/2002GL016452>.
- French, W.J.R., Burns, G.B., 2004. The influence of large-scale oscillations on long-term trend assessment in hydroxyl temperatures over Davis, Antarctica. *J. Atmos. Sol.-Terr. Phys.* 66 (6–9), 493–506.
- Greet, P.A., French, W.J.R., Burns, G.B., Williams, P.F.B., Lowe, R.P., Finlayson, K., 1998. OH(6-2) spectra and rotational temperature measurements at Davis, Antarctica. *Ann. Geophys.* 16, 77–89.
- Jacobi, Ch., Hoffmann, P., Kürschner, D., 2008. Trends in MLT region winds and planetary waves, Collm (52° N, 15° E). *Ann. Geophys.* 26, 1221–1232.
- Khomich, V.Yu., Semenov, A.I., Shefov, N.N., 2008. Airglow as an Indicator of Upper Atmospheric Structure and Dynamics. Springer-Verlag, Berlin/Heidelberg, ISBN: 978-3-540-75832-7.
- Liu, G., Shepherd, G.G., 2006. Perturbed profiles of oxygen nightglow emissions as observed by WINDII on UARS. *J. Atmos. Sol.-Terr. Phys.* 68 (9), 1018–1028.
- López-González, M.J., Rodríguez, E., Wiens, R.H., Shepherd, G.G., Sargoytchev, S., Brown, S., Shepherd, M.G., Aushv, V.M., López-Moreno, J.J., Rodrigo, R., Cho, Y.-M., 2004. Seasonal variations of O₂ atmospheric and OH(6-2) airglow and temperature at mid-latitudes from SATI observations. *Ann. Geophys.* 22, 819–828.
- López-González, M.J., Rodríguez, E., García-Comas, M., Costa, V., Shepherd, M.G., Shepherd, G.G., Aushv, V.M., Sargoytchev, S., 2009. Climatology of planetary wave type oscillations with periods of 2–20 days derived from O₂ atmospheric and OH(6-2) airglow observations at mid-latitude with SATI. *Ann. Geophys.* 27, 3645–3662.
- Lowe, R.P., Turnbull, D.N., 1995. Comparison of ALOHA-93, ANLC-93 and ALOHA-90 observations of the hydroxyl rotational temperature and gravity wave activity. *Geophys. Res. Lett.* 22, 2813–2816.
- McDonald, A.J., Hibbins, R.E., Jarvis, M.J., 2011. Properties of the quasi 16 day wave derived from EOS MLS observations. *J. Geophys. Res.* 116, D06112, <http://dx.doi.org/10.1029/2010JD014719>.
- Mukhtarov, P., Pancheva, D., Andonov, B., 2010. Climatology of the stationary planetary waves seen in the SABER/TIMED temperatures (2002–2007). *J. Geophys. Res.* 115 (A6), A06315, <http://dx.doi.org/10.1029/2009JA015156>.
- Murphy, D.J., French, W.J.R., Vincent, R.A., 2007. Long-period planetary waves in the mesosphere and lower thermosphere above Davis, Antarctica. *J. Atmos. Sol.-Terr. Phys.* 69 (17–18), 2118–2138.

- Offermann, D., Jarisch, M., Oberheide, J., Gusev, O., Wohltmann, I., Russell III, J.M., Mlynczak, M.G., 2006a. Global wave activity from upper stratosphere to lower thermosphere: A new turbopause concept. *J. Atmos. Sol.-Terr. Phys.* 68 (15), 1709–1729, <http://dx.doi.org/10.1016/j.jastp.2006.01.013>.
- Offermann, D., Jarisch, M., Donner, M., Steinbrecht, W., Semenov, A.I., 2006b. OH temperature re-analysis forced by recent variance increases. *J. Atmos. Sol.-Terr. Phys.* 68, 1924–1933.
- Offermann, D., Gusev, O., Donner, M., Forbes, J.M., Hagan, M., Mlynczak, M.G., Oberheide, J., Preusse, P., Schmidt, H., Russell III, J.M., 2009. Relative intensities of middle atmosphere waves. *J. Geophys. Res.* 114, D06110, <http://dx.doi.org/10.1029/2008JD010662>.
- Offermann, D., Hoffmann, P., Knieling, P., Koppmann, R., Oberheide, J., Steinbrecht, W., 2010. Long-term trends and solar cycle variations of mesospheric temperature and dynamics. *J. Geophys. Res.* 115 (D18), D18127, <http://dx.doi.org/10.1029/2009JD013363>.
- Pancheva, D., Mukhtarov, P., Andonov, B., Mitchell, N.J., Forbes, J.M., 2009. Planetary waves observed by TIMED/SABER in coupling the stratosphere-mesosphere-lower thermosphere during the winter of 2003/2004: Part 2—Altitude and latitude planetary wave structure. *J. Atmos. Sol.-Terr. Phys.* 71, 75–87.
- Pancheva, D., Mukhtarov, P., Andonov, B., Forbes, J.M., 2010. Global distribution and climatological features of the 5-6-day planetary waves seen in the SABER/TIMED temperatures (2002–2007). *J. Atmos. Sol.-Terr. Phys.* 72 (1), 26–37.
- Reisin, E.R., Scheer, J., 2004. Gravity wave activity in the mesopause region from airglow measurements at El Leoncito. *J. Atmos. Sol.-Terr. Phys.* 66 (6–9), 655–661.
- Reisin, E.R., Scheer, J., 2009. Evidence of change after 2001 in the seasonal behaviour of the mesopause region from airglow data at El Leoncito. *Adv. Space Res.* 44 (3), 401–412.
- Sassi, F., Garcia, R.R., Boville, B.A., Liu, H., 2002. On temperature inversions and the mesospheric surf zone. *J. Geophys. Res.* 107 (D19), 4380, <http://dx.doi.org/10.1028/2001JD001525>.
- Scheer, J., Reisin, E.R., 2001. Refinements of a classical technique of airglow spectroscopy. *Adv. Space Res.* 27 (6–7), 1153–1158.
- Scheer, J., Reisin, E.R., Espy, J.P., Bittner, M., Graef, H.H., Offermann, D., Ammosov, P. P., Ignatyev, V.M., 1994. Large-scale structures in hydroxyl rotational temperatures during DYANA. *J. Atmos. Terr. Phys.* 56, 1701–1715.
- Scheer, J., Reisin, E.R., Batista, P.P., Clemesha, B.R., Takahashi, H., 2005. Detection of meteor radar wind signatures related to strong short-duration day-to-day airglow transitions at sites 2600 km apart. *J. Atmos. Sol.-Terr. Phys.* 67 (6), 611–621.
- Schmidt, C., Höppner, K., Bittner, M., 2013. A ground-based spectrometer equipped with InGaAs array for routine observations of OH(3–1) rotational temperatures in the mesopause region. *J. Atmos. Sol.-Terr. Phys.* 102, 125–139.
- Shepherd, G.G., Thuillier, G., Cho, Y.-M., Duboin, M.-L., Evans, W.F.J., Gault, W.A., Hersom, C., Kendall, D.J.W., Lathuillière, C., Lowe, R.P., McDade, I.C., Rochon, Y.J., Shepherd, M.G., Solheim, B.H., Wang, D.-Y., Ward, W.E., 2012. The wind imaging interferometer (WINDII) on the upper atmosphere research satellite: a 20 year perspective. *Rev. Geophys.* 50, RG2007, <http://dx.doi.org/10.1029/2012RG000390>.
- Shiokawa, K., Otsuka, Y., Suzuki, S., Katoh, T., Katoh, Y., Satoh, M., Ogawa, T., Takahashi, H., Gobbi, D., Nakamura, T., Williams, B.P., She, C.-Y., Taguchi, M., Shimomai, T., 2007. Development of airglow temperature photometers with cooled-CCD detectors. *Earth Planets Space* 59, 585–599.
- Sigernes, F., Shumilov, N., Deehr, C.S., Nielsen, K.P., Svenøe, T., Havnes, O., 2003. Hydroxyl rotational temperature record from the auroral station in Adventdalen, Svalbard (78° N, 15° E). *J. Geophys. Res.* 108 (A9), 1342, <http://dx.doi.org/10.1029/2001JA009023>.
- Smith, A.K., 2012. Global dynamics of the MLT. *Surv. Geophys.* 33 (6), 1177–1230, <http://dx.doi.org/10.1007/s10712-012-9196-9>.
- Takahashi, H., Wrasse, C.M., Pancheva, D., Abdu, M.A., Batista, I.S., Lima, L.M., Batista, P.P., Clemesha, B.R., Shiokawa, K., 2006. Signatures of 3–6 day planetary waves in the equatorial mesosphere and ionosphere. *Ann. Geophys.* 24, 3343–3350.
- Taylor, M.J., Gardner, L.C., Pendleton Jr., W.R., 2001. Long-period wave signatures in mesospheric OH Meinel (6,2) band intensity and rotational temperature at mid-latitudes. *Adv. Space Res.* 27 (6–7), 1171–1179.
- von Savigny, C., Eichmann, K.-U., Llewellyn, E.J., Bovensmann, H., Burrows, J.P., Bittner, M., Höppner, K., Offermann, D., Taylor, M.J., Zhao, Y., Steinbrecht, W., Winkler, P., 2004. First near-global retrievals of OH rotational temperatures from satellite-based Meinel band emission measurements. *Geophys. Res. Lett.* 31, L15111, <http://dx.doi.org/10.1029/2004GL020410>.
- von Savigny, C., McDade, I.C., Eichmann, K.-U., Burrows, J.P., 2012a. On the dependence of the OH⁺ Meinel emission altitude on vibrational level: SCIAMACHY observations and model simulations. *Atmos. Chem. Phys.* 12, 8813–8828.
- von Savigny, C., Eichmann, K.-U., Robert, C.E., Burrows, J.P., Weber, M., 2012b. Sensitivity of equatorial mesopause temperatures to the 27-day solar cycle. *Geophys. Res. Lett.* 39, L21804, <http://dx.doi.org/10.1029/2012GL053563>.